Lecture 33 Plasmonics: Slab and Gap SPP's

SPP's in thin metal layers

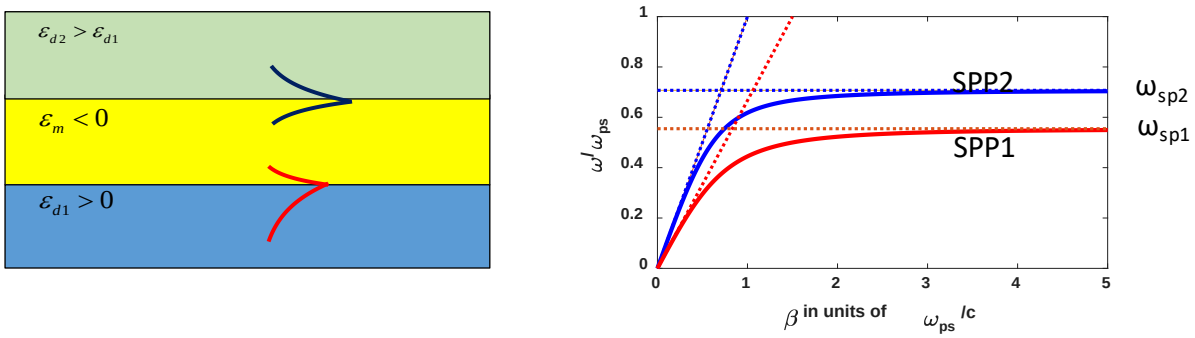

Figure 33.1 (a) SPP's Metal layer between two dielectrics (b) Dispersion of SPP's

Consider a metal layer "sandwiched" between two dielectric cladding layers with different permittivities, $\varepsilon_{d2} > \varepsilon_{d1}$ as shown in Fig. 33.1a. Two SPP's will propagate at each interface and their dispersions are shown in Fig.33. b. Now, the slope of SPP2 dispersion curve at low frequencies is $n_{d2}^{-1} < n_{d1}^{-1}$, while the asymptotic value of frequency (Eq.32.42)

$$\omega_{sp2} = \frac{\omega_{ps}}{\sqrt{\varepsilon_{d2} / \varepsilon_{rb} + 1}} < \omega_{sp1} = \frac{\omega_{ps}}{\sqrt{\varepsilon_{d1} / \varepsilon_{rb} + 1}} \tag{33.1}$$

As metal thickness gets less and less, the two SPP's will become coupled. Let us see what it will lead to.

Slab plasmon waveguide

Consider the situation shown in Fig. 33.2 where we show the symmetric case of the same dielectric on both sides of the metal

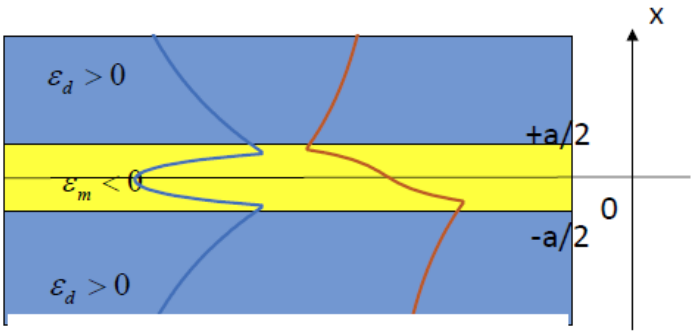

Figure 33.2 Plasmon modes in a metal slab

The situation is expected to be simialr to the dielectric waveguide, but since the dielectric constant of metal is negative we shall have hyperbolic cosine and sine for even and odd modes. So, inside the metal we can write

$$H_y(|x|<\frac{a}{2})=\begin{cases}H_0\cosh(q_m x)e^{j(\beta z-\omega t)}\\ H_0\sinh(q_m x)e^{j(\beta z-\omega t)}\end{cases}\quad q_m=\sqrt{|\varepsilon_m|k_0^2+\beta^2} \tag{33.2}$$

In the cladding we have the same situation as in dielectric waveguides

$$H_y(|x|>\frac{a}{2})=\begin{cases}H_0\cosh\frac{q_d a}{2}e^{-q_d(|x|-a/2)}e^{j(\beta z-\omega t)}\\ H_0\sinh\frac{q_d a}{2}e^{-q_d(|x|-a/2)}e^{j(\beta z-\omega t)}\end{cases}\quad q_d=\sqrt{\beta^2-\varepsilon_d k_0^2} \tag{33.3}$$

The same condition (32.30) relates the transverse decay constants

$$q_m^2-q_d^2=\left(|\varepsilon_m|+\varepsilon_d\right)k_0^2 \tag{33.4}$$

Let us find the longitudinal electric field according to Eq. 32.25 for even mode

$$E_z=\frac{j}{\omega\varepsilon_0\varepsilon_r(x)}\frac{\partial H_y}{\partial x}=\begin{cases}\frac{jq_m H_0 e^{j(\beta z-\omega t)}}{\omega\varepsilon_0\varepsilon_m}\sinh q_m x & |x|<a/2\\ -\frac{jq_d H_0 e^{j(\beta z-\omega t)}e^{-q_d x}}{\omega\varepsilon_0\varepsilon_d}\cosh q_m\frac{a}{2} & x>a/2\end{cases} \tag{33.5}$$

and

$$E_z=\frac{j}{\omega\varepsilon_0\varepsilon_r(x)}\frac{\partial H_y}{\partial x}=\begin{cases}\frac{jq_m H_0 e^{j(\beta z-\omega t)}}{\omega\varepsilon_0\varepsilon_m}\cosh q_m x & |x|<a/2\\ -\frac{jq_d H_0 e^{j(\beta z-\omega t)}e^{-q_d x}}{\omega\varepsilon_0\varepsilon_d}\sinh q_m\frac{a}{2} & x>a/2\end{cases} \tag{33.6}$$

for odd mode. The continuity of E_z leads to

$$\frac{q_m\sinh(q_m a/2)}{q_d\cosh(q_m a/2)}=-\frac{\varepsilon_m}{\varepsilon_d}=\frac{|\varepsilon_m|}{\varepsilon_d} \tag{33.7}$$

for even mode. Introduce, as in dielectric waveguides

$$u=q_m a/2;\ v=q_d a/2 \tag{33.8}$$

The boundary condition (33.7) becomes

$$v = \frac{\varepsilon_d}{|\varepsilon_m|} u \tanh u \tag{33.9}$$

for even mode, and, of course,

$$v = \frac{\varepsilon_d}{|\varepsilon_m|} \frac{u}{\tanh u} \tag{33.10}$$

for odd mode. Next, re-writing (33.4) as

$$u^2 - v^2 = \left(|\varepsilon_m| + \varepsilon_d\right) k_0^2 a^2 / 4 = \left(1 + \frac{\varepsilon_d}{|\varepsilon_m|}\right) w^2, \tag{33.11}$$

where we introduce

$$w = k_0 |\varepsilon_m|^{1/2} a / 2 = \frac{a}{2L_{skin}} \approx \frac{\omega}{c} \frac{\omega_p}{\omega} \frac{a}{2} = \frac{\pi a}{\lambda_p} \tag{33.12}$$

In Au and Ag $\lambda_p \sim 140 - 150nm$ so the skin depth is

$$L_{skin} = 1/|\varepsilon_m|^{1/2} k_0 \approx \lambda_p / 2\pi \approx 25nm \tag{33.13}$$

We can now proceed with the graphic solution for the case of gold on glass, $\lambda = 750nm$, $\varepsilon_m = -20$ and $\varepsilon_d = 2.25$ This is done in Fig.33.3 First we plot (33.9) which goes through the origin of coordinates(33.9), then which does not go through origin since $u / \tanh u \to 1$ for small u. Next we plot (33.11) – set of hyperbolas for different normalized metal thicknesses w. We immediately observe that the odd solution always has larger *v* than even solution. *Therefore, the even solution spreads more into dielectric and has lower loss than odd solution, which is well confined to the meta, therefore even solution has longer propagation range.*

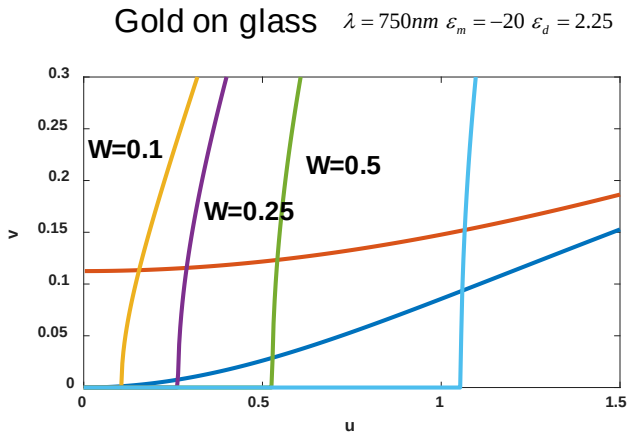

Figure 33.3 Graphic solution for the modes of slab plasmon

As long as $\varepsilon_d / |\varepsilon_m| << 1$ one can say that

$$u >> v \approx \sqrt{1+\frac{\varepsilon_d}{|\varepsilon_m|}} w \approx w \tag{33.14}$$

Then for even mode according to (33.9)

$$v_{even} = \frac{\varepsilon_d}{|\varepsilon_m|} w \tanh w \approx \frac{\varepsilon_d}{|\varepsilon_m|} w^2 << u \tag{33.15}$$

It follows from (33.8) then that as long as $a << \lambda_0$

$$q_{d,even} \approx \frac{2}{a}\frac{\varepsilon_d}{|\varepsilon_m|} w^2 = \frac{2}{a}\frac{\varepsilon_d}{|\varepsilon_m|} k_0^2 |\varepsilon_m| \frac{a^2}{4} = k_0 n_d \frac{k_0 n_d a}{2} << k_0 n_d \tag{33.16}$$

The propagation constant of even mode is according to (33.3)

$$\beta_{even}^2 = \varepsilon_d k_0^2 + q_{d,even}^2 \approx n_d^2 k_0^2 (1 + n_d^2 k_0^2 a^2 / 4), \tag{33.17}$$

i.e. it is not much different from the wavevector in dielectric indicating that the wave is mostly propagating in the dielectric.

The odd mode, on the other hand has roughly the same

$$v_{odd} = \frac{\varepsilon_d}{|\varepsilon_m|} > v_{even} \tag{33.18}$$

Nearly independent of metal thickness. The decay constant in dielectric is

$$q_{d,odd} \approx \frac{2}{a}\frac{\varepsilon_d}{|\varepsilon_m|} = \frac{k_0 n_d}{w}\left(\frac{\varepsilon_d}{|\varepsilon_m|}\right)^{1/2} > k_0 n_d > q_{d,even} \tag{33.19}$$

The propagation constant of the odd mode is then

$$\beta_{odd} = \sqrt{\varepsilon_d^2 k_0^2 + q_{d,odd}^2} \approx q_{d,odd} \approx \frac{2}{a}\frac{\varepsilon_d}{|\varepsilon_m|} \tag{33.20}$$

i.e. it increases with the decrease of the thickness.

Slab plasmon characteristics

The even (long range) and odd (short range) plasmon characteristics are shown in Fig.33.4. First, in Fig.33.4a the dependence of propagation constant on metal thickness is shown. For thick metal layers two curves merge – meaning that one simply has two SPP's on two surfaces that are not coupled, but as thickens sis reduced to skin depth and less the modes split – the even mode propagation constant gets smaller as the field escapes into the dielectric (that is also seen in the dependence of penetration depth

into dielectric $1/q_d$ shown in Fig. 33.4b. For the odd mode the propagation constant increases with decrease of thickness. The magnetic field of two modes is shown in Fig.33.4 c and d for two different thicknesses. As one can see for 100nm thick metal the odd and even modes penetrate the dielectric by about the same amount, but for 30nm case the even mode spreads much further.

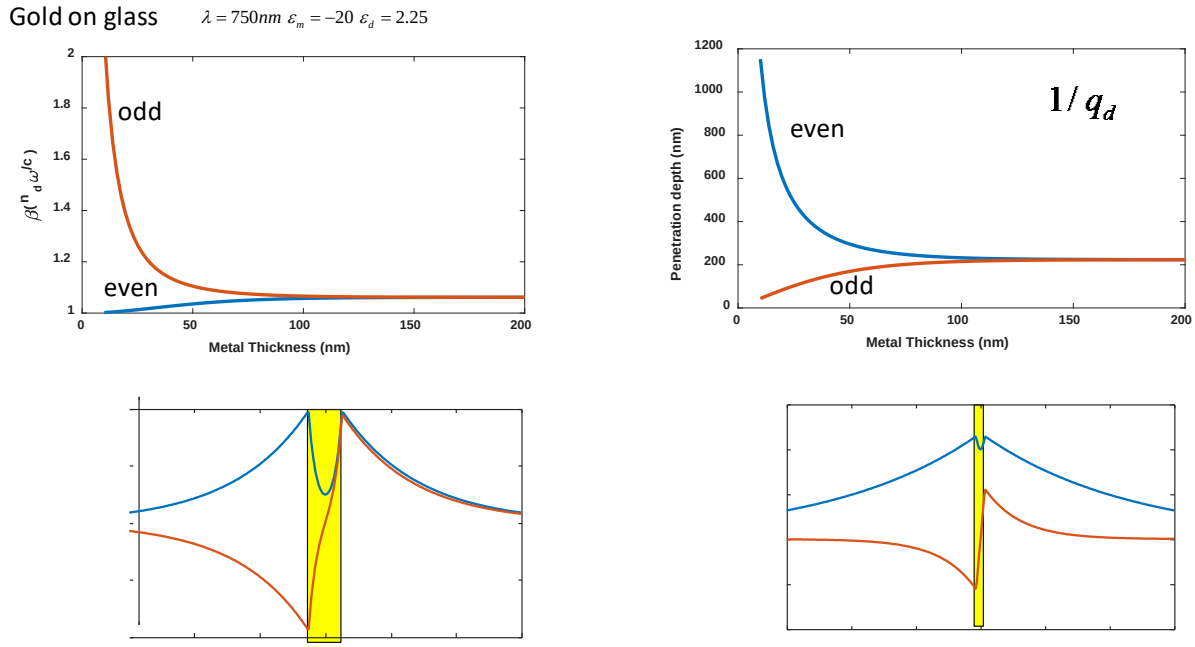

Figure 33.4 Plasmon modes in a gold slab (a) propagation constant vs. metal thickness (b) Penetration into the metal depth vs. metal thickness (c,d) Magnetic field in the odd and even modes for different thicknesses.

In Fig 33.5 (a) one can see the dispersion of slab plasmons for $a = 12nm$ - clearly the odd mode has much larger propagation constant than even mode. Fig.33.5 b depicts the penetration depth as a function of frequency and Fig.33.5 c shows the transverse electric field - - the field is more tightly confined in tehmetal for odd mode, hence it bears the name of a "short range plasmon".

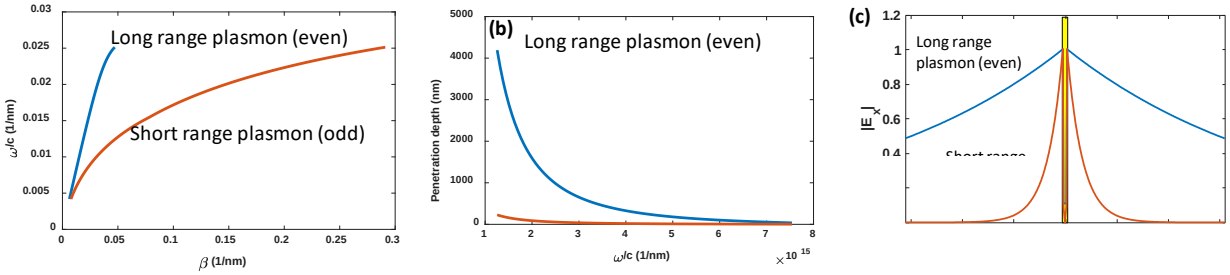

Figure 33.5 (a) dispersion of slab SPP's (b) Penetration depth vs frequency (c0 Transverse electric field

In Fig.33.6 various applications of slab plasmons are shown – - from information transmission to sensing to modulation/attenuation.

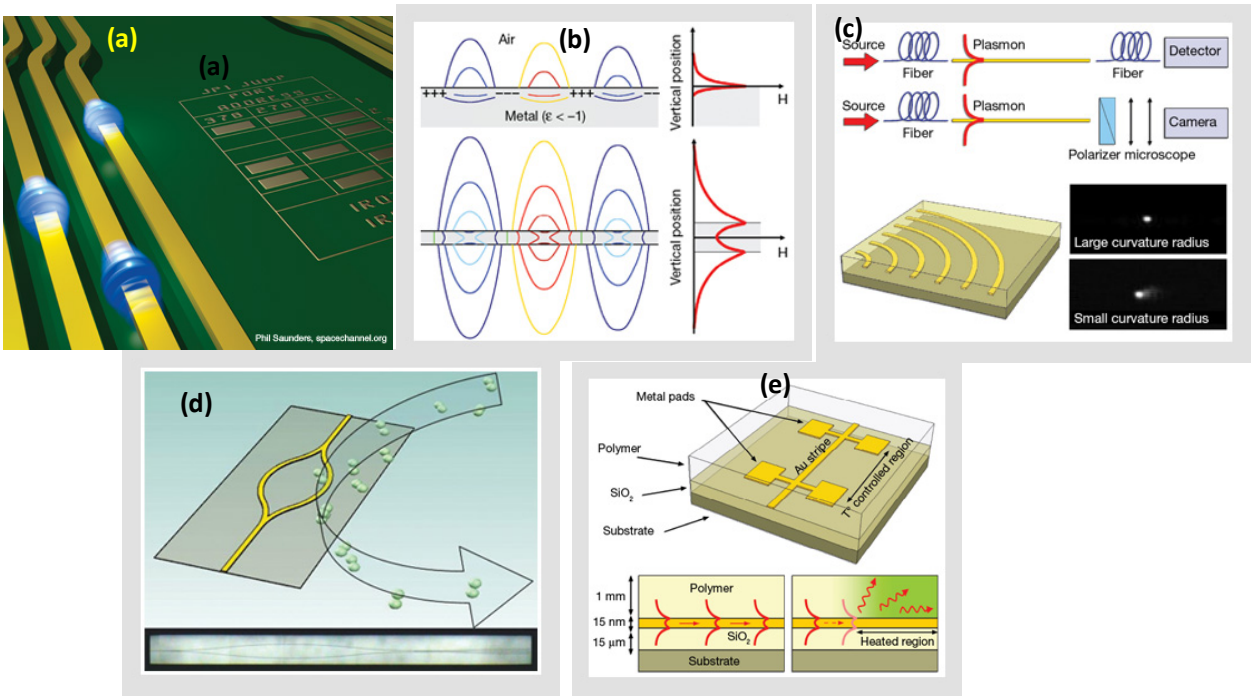

Figure 33.6 Applications of slab SPP's (a-c) transmission liens (d) sensing (e) attenuator

The thermo-optic attenuator depicted in Fig. 33.6 e consists of a metal stripe sandwiched between a layer of SiO2 and a polymer having different thermo-optic properties. At room temperature, the long-range plasmon can propagate because the chosen polymer is index-matched to SiO_2. When the temperature rises, the index of the polymer becomes different than that of the SiO_2. The resulting asymmetry strongly attenuates the mode, which becomes radiative.

Gap (or slot) plasmons

Let us now consider the situation reversed to the slab plasmon, i.e. a dielectric (often the air) core sandwiched between metal cladding as shown in Fig. 33.7

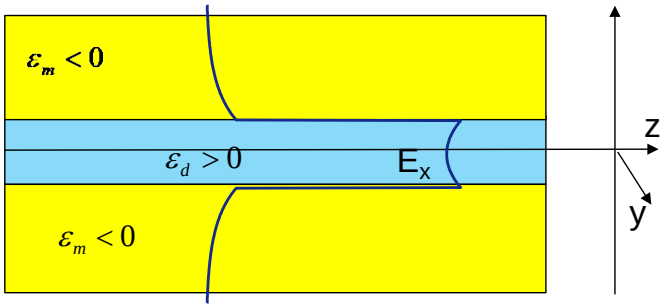

Figure 33.7 Gap plasmon and transverse electric field in it

The transverse magnetic field inside the dielectric gap is

$$H_y(|x|<\frac{a}{2})=\begin{cases}H_0\cosh(q_d x)e^{j(\beta z-\omega t)}\\ H_0\sinh(q_d x)e^{j(\beta z-\omega t)}\end{cases}\quad q_d=\sqrt{\beta^2-\varepsilon_d k_0^2}, \tag{33.21}$$

For even and odd modes, respectively, and in the metal cladding it is

$$H_y(|x|>\frac{a}{2})=\begin{cases}H_0\cosh\frac{q_d a}{2}e^{-q_m(|x|-a/2)}e^{j(\beta z-\omega t)}\\ H_0\sinh\frac{q_d a}{2}e^{-q_m(|x|-a/2)}e^{j(\beta z-\omega t)}\end{cases}\quad q_m=\sqrt{|\varepsilon_m|k_0^2+\beta^2}, \tag{33.22}$$

while (33.4) still stands as

$$q_m^2-q_d^2=\left(|\varepsilon_m|+\varepsilon_d\right)k_0^2 \tag{33.23}$$

Once again, let us find the longitudinal electric field of the even mode

$$E_z=\frac{j}{\omega\varepsilon_0\varepsilon_r(x)}\frac{\partial H_y}{\partial x}=\begin{cases}\frac{jq_d H_0 e^{j(\beta z-\omega t)}}{\omega\varepsilon_0\varepsilon_d}\sinh q_d x & |x|<a/2\\ -\frac{jq_m H_0 e^{j(\beta z-\omega t)}e^{-q_d x}}{\omega\varepsilon_0\varepsilon_m}\cosh q_d\frac{a}{2} & x>a/2\end{cases} \tag{33.24}$$

The continuity of this field at the boundary leads to the boundary condition

$$\frac{q_d\sinh\left(q_d a/2\right)}{q_m\cosh\left(q_d a/2\right)}=-\frac{\varepsilon_d}{\varepsilon_m}=\frac{\varepsilon_d}{|\varepsilon_m|}, \tag{33.25}$$

which, upon introduction of dimensionless parameters $u=q_d a/2;\ v=q_m a/2$ as in (33.8) results in

$$v=\frac{|\varepsilon_m|}{\varepsilon_d}u\tanh u, \tag{33.26}$$

which is just (33.9) with metal and dielectric permittivities exchanging places. Easy to see that for off mode one gets

$$v=\frac{|\varepsilon_m|}{\varepsilon_d}\frac{u}{\tanh u} \tag{33.27}$$

Introducing the normalized width in analogy with (33.11) but this time changing the sign, since according to (33.23) $v>u$ we have

$$u^2-v^2=-\left(|\varepsilon_m|+\varepsilon_d\right)k_0^2a^2/4=-\left(1+\frac{\varepsilon_d}{|\varepsilon_m|}\right)w^2 \tag{33.28}$$

where just as in (33.12)

$$w = k_0 \,|\, \varepsilon_m \,|^{1/2}\, a/2 = \frac{a}{2L_{skin}} \approx \frac{\omega}{c}\frac{\omega_p}{\omega}\frac{a}{2} = \frac{\pi a}{\lambda_p} \tag{33.29}$$

We now proceed with the graphic solution as shown in Fig.33.8 a. for the case of gold with air gap, $\lambda = 750nm\ \varepsilon_m = -20\ \varepsilon_d = 1.$ First thing we notice that while the even solution (33.26) starts in the origin of coordinates, for odd (33.27) solution starts at $v = |\varepsilon_m| / \varepsilon_d >> 1$. The plots of (33.28) for different a's are hyperbolas and since $w = a/2L_{skin} \approx a/50nm$ is typically less than 1, these plots are all very close to the horizontal axis, hence, one must conclude, that the *odd solution simply does not exist.*

In order to see the even solution, one has to zoom in as shown in Fig.33.8b.

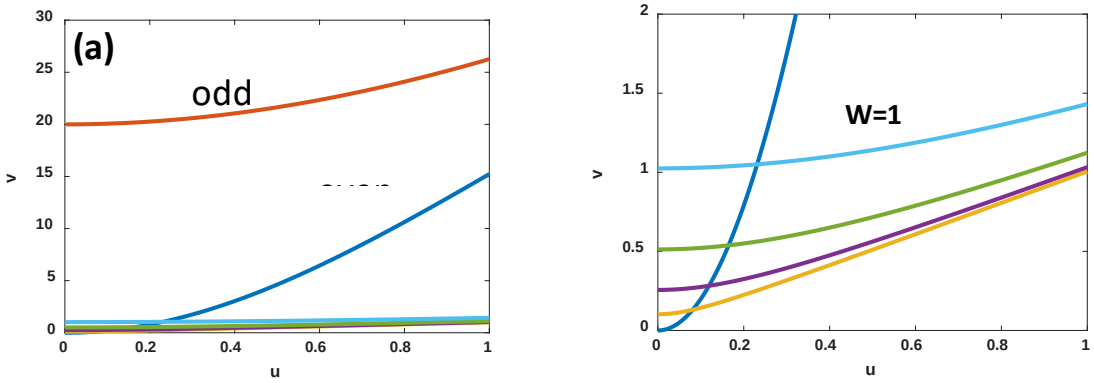

Figure 33.8 (a) Graphic solution for gap plasmon (b) its zoom.

As one can see now the curve (33.26) starts as

$$v \approx \frac{|\varepsilon_m|}{\varepsilon_d} u^2 \tag{33.30}$$

and for $\varepsilon_d / |\varepsilon_m| << 1$, and for w's that are not outrageously small ($a > L_{skin}$) the solution $v >> u$ and according to (33.28).

$$\begin{aligned} v &\approx w \\ u &\approx \sqrt{\frac{\varepsilon_d}{|\varepsilon_m|} w} \end{aligned} \tag{33.31}$$

We then obtain

$$q_m \approx \frac{2}{a} w = \frac{2\pi}{\lambda_p} = \frac{1}{L_{skin}} \tag{33.32}$$

which is of course an expected result – the field decays over the skin depth in the metal. Also

$$q_d \approx \frac{2}{a}\sqrt{\frac{\varepsilon_d}{|\varepsilon_m|} w} = \frac{2}{a}\sqrt{\frac{\varepsilon_d}{|\varepsilon_m|} k_0 \,|\, \varepsilon_m \,|^{1/2}\, \frac{a}{2}} = n_d k_0 \sqrt{\frac{1}{|\varepsilon_m|^{1/2}} \frac{2}{a k_0}} = n_d k_0 \sqrt{1/w} \tag{33.33}$$

And finally substituting (33.33) into (33.21) we obtain the expression for the propagation constant

$$\beta^2 = \varepsilon_d k_0^2 + q_d^2 \approx n_d^2 k_0^2 \left(1 + \frac{\lambda_p}{\pi a}\right)$$
$$\beta \approx n_d k_0 \left(1 + \frac{\lambda_p}{2\pi a}\right) \tag{33.34}$$

The effective index of the gap plasmon mode is

$$n_{eff} = \beta / k_0 \approx n_d \left(1 + \frac{\lambda_p}{2\pi a}\right) \tag{33.35}$$

and it has a very weak frequency dependence for as long as gap is larger than skin depth. The mode is very well confined inside the dielectric.

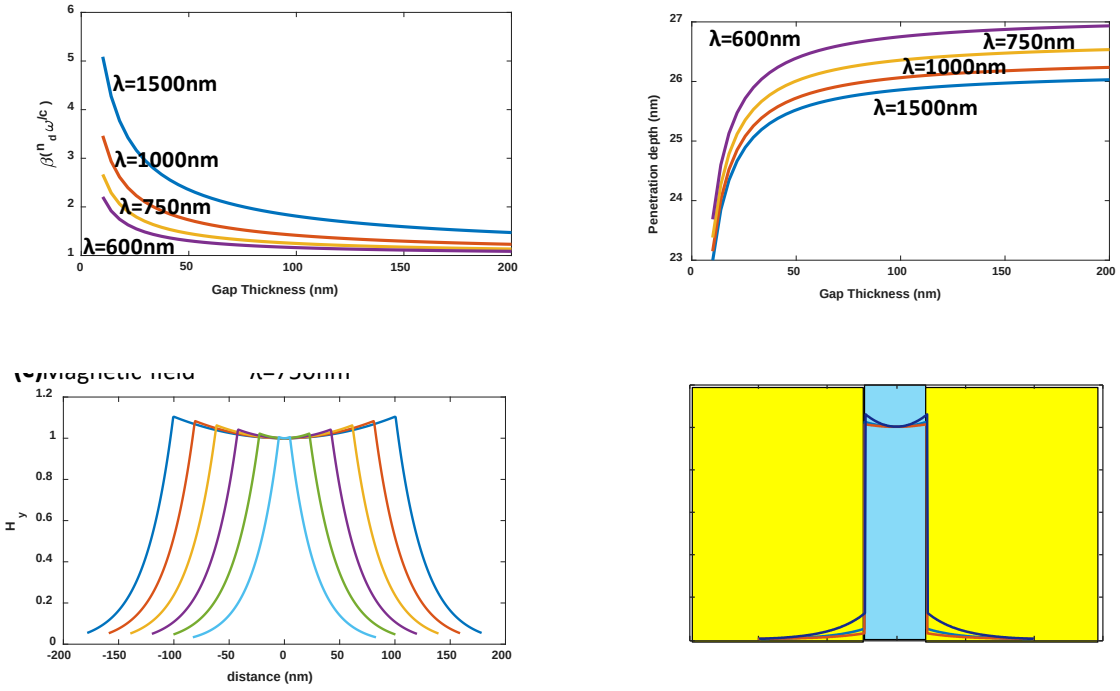

Figure 33.9 Gap plasmons (a) Effective index (relative to dielectric) and (b) metal penetration depth vs gap thickness for different wavelengths (c) magnetic field for different gap thicknesses and $\lambda = 750nm$ (d) electric field for different waveelngths

All of these observations are evident in Fig.33.9- as shown in Fig.33.9a for large range of gap thicknesses effective index remains very close to the index of dielectric, the penetration depth (Fig.33.9b) remains equal to the skin depth in the metal and – both magnetic (Fig.33.9c) and electric (Fig.33.9d) fields are confined inside the dielectric. For al practical purposes this is a standard TEM (transverse electro-magnetic) wave in a metal transmission line –it has very little to do with a "real" plasmon.

Higher order solutions

The question arises, are there solutions (especially the odd ones)?. For that consider a case when the field inside the dielectric has real transverse wavevector (as shown in Fig.39.10) and the effective index is less than refractive index of the dielectric.

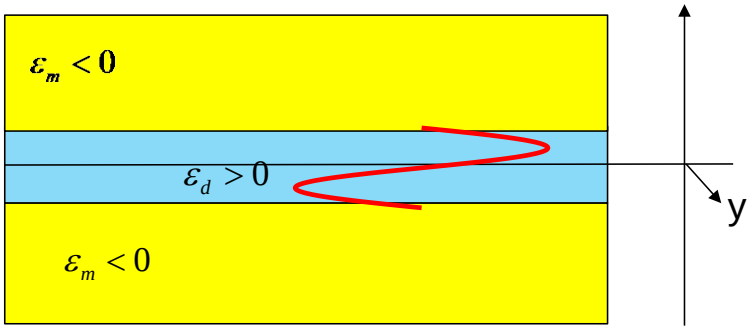

Figure 33.10 Odd mode in the metal lot waveguide

$$H_y(|x|<\frac{a}{2}) = \begin{cases} H_0 \cos(q_d x) e^{j(\beta z-\omega t)} \\ H_0 \sin(q_d x) e^{j(\beta z-\omega t)} \end{cases} \quad q_d = \sqrt{\varepsilon_d k_0^2 - \beta^2}, \tag{33.36}$$

for even and odd modes respectively. In the metal cladding we still have evanescent waves

$$H_y(|x|>\frac{a}{2}) = \begin{cases} H_0 \cos\frac{q_d a}{2} e^{-q_m(|x|-a/2)} e^{j(\beta z-\omega t)} \\ H_0 \sin\frac{q_d a}{2} e^{-q_m(|x|-a/2)} e^{j(\beta z-\omega t)} \end{cases} \quad q_m = \sqrt{|\varepsilon_m| k_0^2 + \beta^2} \tag{33.37}$$

One can see that

$$q_m^2 + q_d^2 = \left(|\varepsilon_m| + \varepsilon_d\right) k_0^2 \tag{33.38}$$

The longitudinal electric field in even mode

$$E_z = \frac{j}{\omega\varepsilon_0\varepsilon_r(x)}\frac{\partial H_y}{\partial x} = \begin{cases} -\frac{jq_d H_0 e^{j(\beta z-\omega t)}}{\omega\varepsilon_0\varepsilon_d}\sin q_d x & |x|<a/2 \\ -\frac{jq_m H_0 e^{j(\beta z-\omega t)} e^{-q_d x}}{\omega\varepsilon_0\varepsilon_m}\cos q_d\frac{a}{2} & x>a/2 \end{cases} \tag{33.39}$$

and its continuity at the boundary implies that for even mode

$$\frac{q_d \sin\left(q_d a/2\right)}{q_m \cos\left(q_d a/2\right)} = \frac{\varepsilon_d}{\varepsilon_m} = -\frac{\varepsilon_d}{|\varepsilon_m|} \tag{33.40}$$

Once again introducing $u = q_d a/2;\ v = q_m a/2$ we obtain

$$v_{even} = -\frac{|\varepsilon_m|}{\varepsilon_d} u \tan u, \tag{33.41}$$

and for odd mode

$$v_{odd} = \frac{|\varepsilon_m|}{\varepsilon_d}\frac{u}{\tan u} = -\frac{|\varepsilon_m|}{\varepsilon_d} u \tan(u + \pi/2) \tag{33.42}$$

and using (33.29) we also obtain from (33.38)

$$u^2 + v^2 = \left(|\varepsilon_m| + \varepsilon_d\right) k_0^2 a^2/4 = \left(1 + \frac{\varepsilon_d}{|\varepsilon_m|}\right) w^2, \tag{33.43}$$

Equation of a circle. Let us do graphic solution as in Fig. 33.11a First thing we note that for the first even solution TM) simply does not exist because v is always negative – instead of it one has TEM wave – a very special solution. Since $|\varepsilon_m|/\varepsilon_d >> 1$ the graphs of (33.41) and (33.42) are practically vertical lines going through $u_m = m\pi/2$ indicating that solution for m-th mode is $q_{d,m} = m\pi/a$ indicating round trip phase delay of $2m\pi$ - Fabry-Perot resonance. Of course, not every intersection in Fig.33.11a is real solution since according to (33.36) $\beta = \sqrt{\varepsilon_d k_0^2 - q_d^2}$, must be real hence $m\pi/a \le n_d k_0$ and maximum m is

$$m_{\max} = Int(k_0 a n_d/\pi) = Int(2a n_d/\lambda_0) \tag{33.44}$$

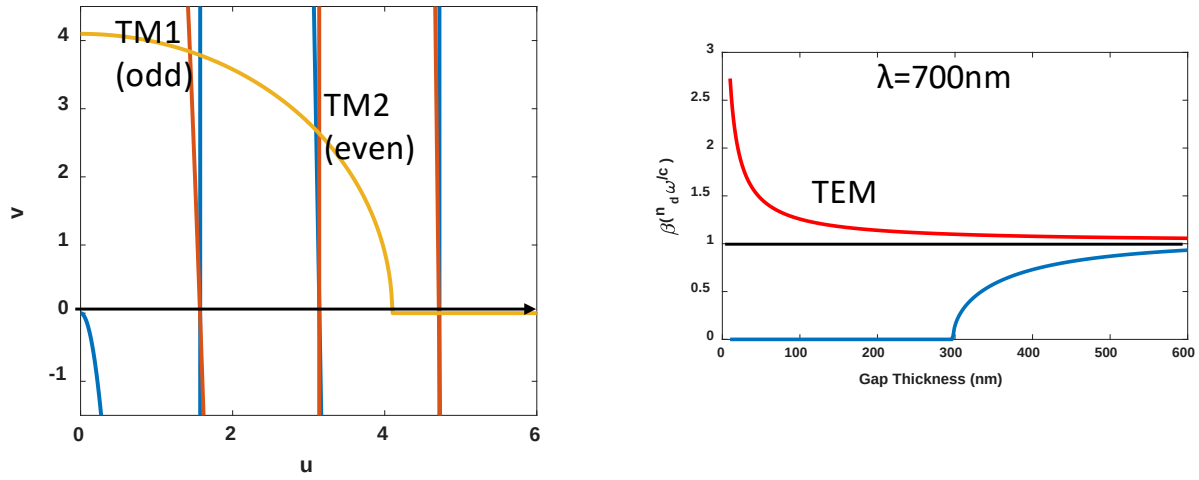

Figure 33.11 (a) graphic solution for higher TM modes in slot waveguide(b) effective index vs. gap width

The dependence of effective index of TEM and TM1 modes is shown in Fig.33.11b. TM1, unlike TEM experiences cutoff, obviously when $a < \lambda_0/2n_d$ The effective index of TM1 and higher order modes is less than n_d - because the light propagates at an angle to the axis.

Applications of gap plasmons

Gap plasmons have been investigated for use in future interconnects as shown in Fig.33.12

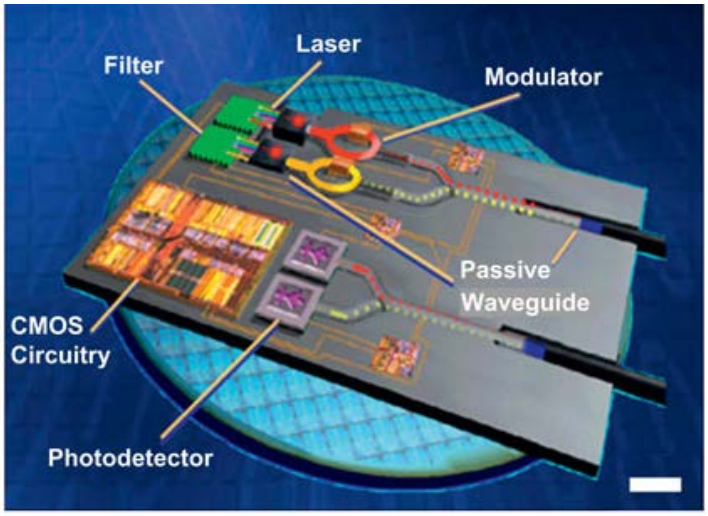

Figure 33.12 Plasmonic interconnects

There exist many variations of gap plasmons and slab plasmons as shown in Fig. 33.13. Also popular are the hybrid plasmon polaritons (HPP) where part of the confinement is provided by metal, but most of light is confined by index contrast just as in a normal dielectric waveguide

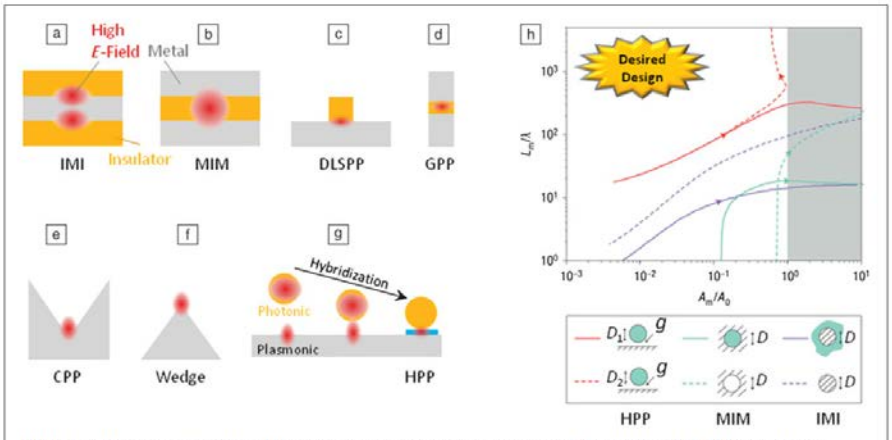

Figure 2. Surface plasmon waveguide architectures. Shown are the waveguide cross-sections, with the optical data propagating in the third dimension. (a) Insulator-metal-insulator (IMI),[15] (b) metal-insulator-metal (MIM),[16] (c) dielectric loaded surface plasmon polariton (DLSPP),[22–24] (d) gap plasmon polariton (GPP),[19] (e) channel plasmon polariton (CPP),[18] (f) wedge SPP,[20] and (g) hybrid plasmon polariton (HPP).[17,25,26] (h) A figure-of-merit comparison for nanoscale waveguides (HPP, IMI, MIM) highlights the achievable propagation distance (L_m) in numbers of operation wavelength, λ, to the propagating optical mode size, A_m, normalized by the diffraction limit of light, $A_0 = \lambda^2/4$.[26] A trajectory shows a range of one structural parameter: HPP gap g = [1, 10^4] nm and core diameters D_1 = 200 nm, D_2 = 215 nm; for IMI and MIM D = [10, 10^4] nm (red curves). Scaling D of the MIM mode introduces an optical mode cutoff (green curves). The IMI does not suffer from a cutoff, yet the propagation lengths are limited (blue curves). The HPP mode offers both strong optical confinement and reasonably long propagation performance. The gray area highlights mode sizes that are above the diffraction limit. Dashed versus solid curves for IMI and MIM show dielectric (green) versus air cladding (white), respectively. Material relative permittivity: semiconductor = GaAs (ε_s = 12.25), oxide = SiO_2 (ε_{ox} = 2.25), metal = Ag (ε_m = −129 + 3.3i), and λ = 1550 nm. Note: *E*-field, electric field.

Figure 33.13 Surface plasmon polariton architectures.

The comparative characteristics of different SPP architectures are shown in Table 33.1. As one can see as mode confinement gets stronger loss increases.

Table I. Plasmonic waveguide comparison of optical confinement (mode area) and propagation length (L_m) from the literature, λ free-space wavelength.

Waveguide Type	Mode Width/λ	Mode Height/λ	Mode Area/(λ/2)²	L_m/λ	λ (nm)	Ref.
GPP	0.13	0.13	7%	13	1550	19
Wedge	~0.47	N.A.	N.A.	2	633	20
MIM	0.5	0.2	10%	5	685	16
IMI	0.19	~0.19	~14%	14	1550	15
CPP (V–groove)	0.65	>0.84 Groove depth = 1.3 μm	>200%	~52	1550	18
DLSPP	0.62	N.A.	N.A.	10	800	22
DLSPP	N.A.	N.A.	3%	4	1550	23
HPP	0.04	0.04	0.6%	21	1550	26
	0.14	0.04	2%	N.A.	1427	17
	0.31	0.06	7%	21	808	17
	0.09	0.08	3%	11	633	17
	$0.15_{(Theory)}$	$0.05_{(Theory)}$	3%	24	1310	7

GPP, gap plasmons; Wedge, plasmon polaritons; MIM, metal-insulator-metal; IMI, insulator-metal-insulator; CPP, channel plasmon polariton; DLSPP, dielectric loaded surface plasmon polariton; HPP, hybrid plasmon polariton; N.A., not available.

Table 33.1 Confinement vs loss in SPP

Important prospective applications are plasmonic nanolasers as shown in Fig.33.14

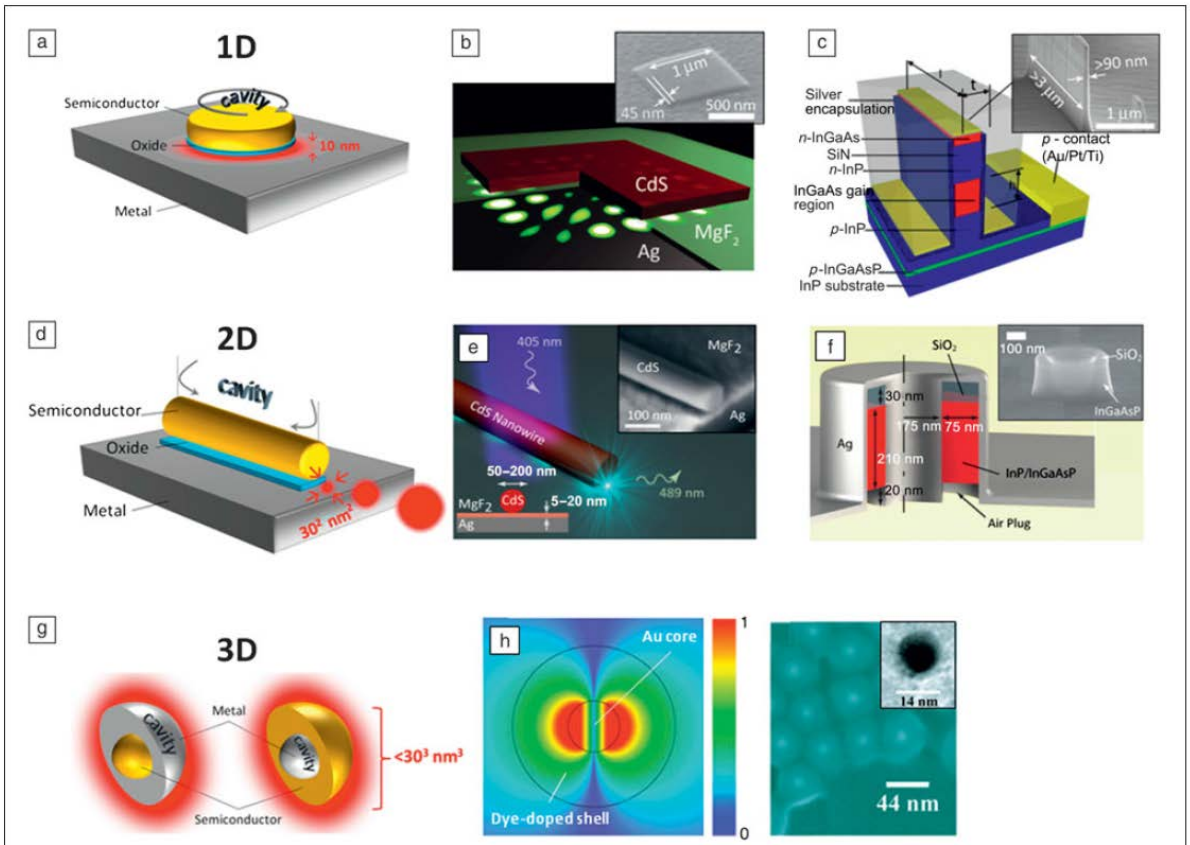

Figure 4. Plasmon nanolasers with different levels of optical confinement beyond the diffraction limit of light. (a–c) 1D plasmonic optical confinement. (b) Plasmon nanolaser featuring an in-plane cavity and total internal reflection of the resonating mode.[39,40] (c) Fabry–Pérot type plasmon laser as a wall-like post.[41] (d–f) 2D plasmon optical confinement showing (e) a Fabry-Perot type resonator utilizing the HPP mode[38] and (f) a coaxial type resonator.[42] (g) Two possible configurations of a spatially localized resonator featuring 3D optical confinement. (h) Localized plasmon laser demonstration utilizing a (14 nm) gold core surrounded by an Oregon Green (OG 488 nm) dye-doped silica shell. The left panel showing the electric field intensity (unity normalized) of the particle resonator indicates a strongly localized field at the metal particle (red area).[43]

Figure 33.14. Plasmonic nanolasers

And plasmonic light modulators as shown in Fig.33.15

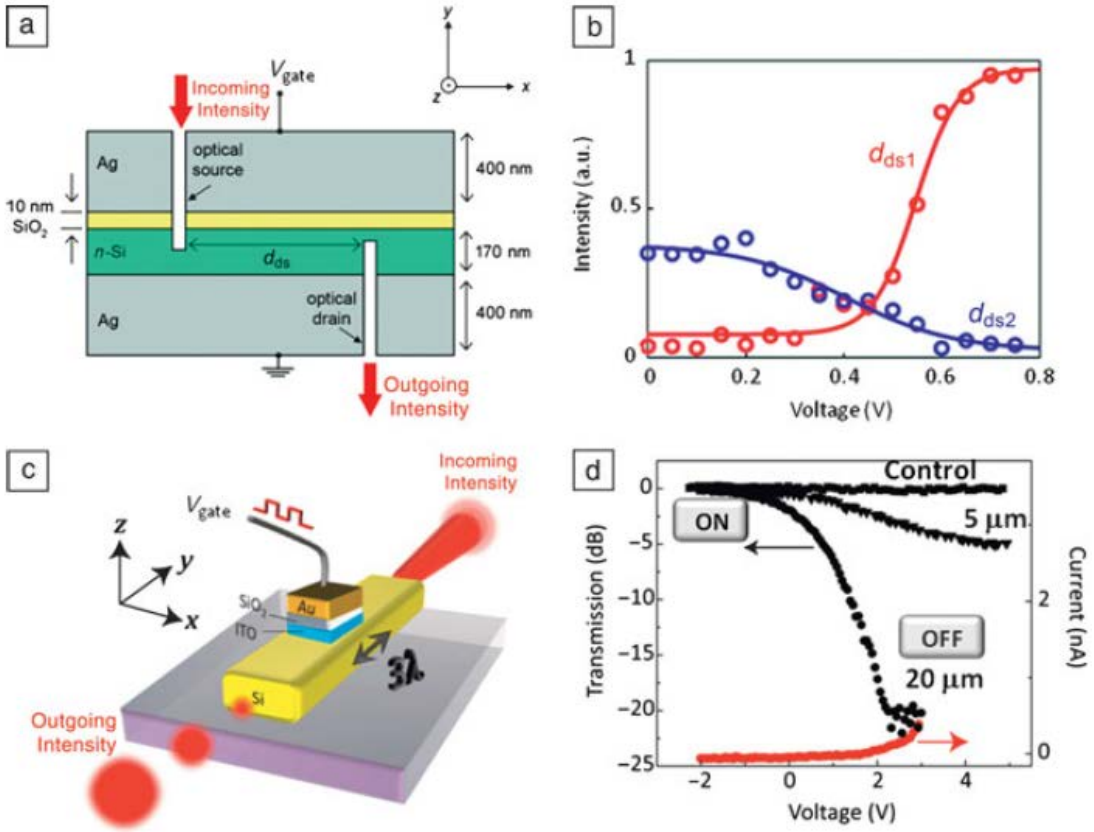

Figure 33.15 Miniature plasmonic modulators